

Quantum many-body spin rings coupled to ancillary spins: The sunburst quantum Ising modelAlessio Franchi , Davide Rossini, and Ettore Vicari *Dipartimento di Fisica, Università di Pisa and INFN, Largo Pontecorvo 3, 56127 Pisa, Italy*

(Received 24 February 2022; accepted 20 April 2022; published 5 May 2022)

We study the ground-state properties of a quantum sunburst model, composed of a quantum Ising spin ring in a transverse field, symmetrically coupled to a set of ancillary isolated qubits, to maintain a residual translation invariance and also a \mathbb{Z}_2 symmetry. The large-size limit is taken in two different ways: either by keeping the distance between any two neighboring ancillary qubits fixed or by fixing their number while increasing the ring size. Substantially different regimes emerge, depending on the various Hamiltonian parameters: For small energy scale δ of the ancillary subsystem and small ring-qubit interaction κ , we observe rapid and nonanalytic changes in proximity to the quantum transitions of the Ising ring, both first order and continuous, which can be carefully controlled by exploiting renormalization-group and finite-size scaling frameworks. Smoother behaviors are instead observed when keeping $\delta > 0$ fixed and in the Ising disordered phase. The effect of an increasing number n of ancillary spins turns out to scale proportionally to \sqrt{n} for sufficiently large values of n .

DOI: [10.1103/PhysRevE.105.054111](https://doi.org/10.1103/PhysRevE.105.054111)**I. INTRODUCTION**

The recent amazing progress on the control of physical systems at the nanoscale has paved the way toward deep investigations of quantum properties of matter and the more complex problem of monitoring the coherent quantum dynamics of mutually coupled systems, addressing energy interchanges and the relative decoherence properties among the various subsystems [1]. These issues are relevant both for fundamental reasons, such as to improve our understanding of the emergence of interference and entanglement useful for quantum-information purposes [2] or for enhancing the efficiency of energy conversion in complex networks [3], and for more applied quantum-thermodynamical purposes, such as the optimization of energy storage in subportions of the whole system [4] or the realization of work extraction engines at the nanoscale [5]. The possible presence of different quantum phases and the development of criticality in the system may be exploited to characterize the sensitivity to a variety of behaviors [6].

From a conceptual point of view, the cleanest scenario is perhaps that of a system composed of several quantum objects described by a global static Hamiltonian. A portion of the system itself can thus be seen as an effective bath for the remaining part. In this context, paradigmatic toy models are the so-called central-spin models [for a sketch, see Fig. 1(a)], where one or a few qubits are globally coupled to an environmental many-body system (see, e.g., Refs. [7–20]). The main decoherence properties of a single qubit (red dot) globally coupled to a many-body system (surrounding blue dots) turn out to crucially depend on the quantum phase of the many-body system, whether it is within the ordered or disordered quantum phases, or at the quantum critical

point (QCP) separating them, when it develops long-range correlations [20].

Here we return to issues related to the decoherence arising from interactions between different parts of an isolated system and propose an alternative arrangement of its composing quantum objects, which we call the sunburst model [a sketch is shown in Fig. 1(b)]. Namely, we consider a quantum spin chain (blue dots) locally coupled to external isolated qubits (surrounding red dots). The sunburst model admits a high degree of flexibility in the choice of the number of external qubits, which can be a finite or an infinite set at regular spatial intervals, and may be interpreted as a probing subsystem. The specific geometry of the model makes it nonintegrable, apart from very specific cases; therefore, numerical approaches are usually needed to study the emerging physics.

In this paper we study the case in which the inner ring is described by a quantum Ising chain, being a prototypical quantum many-body system which presents different quantum phases, with both first-order quantum transitions (FOQTs) and continuous quantum transitions (CQTs) when varying the intensity of the two external, transverse and longitudinal, fields. In this exploratory study of the sunburst quantum Ising model, we investigate the equilibrium properties of the ground state of the global system, focusing on the behavior of observables associated with the Ising chain or the ancillary qubits separately. This allows us to address the effects of interactions between the two parts on the coherence properties of the single part, and the scaling behaviors associated with the different phases of the Ising system. Close to the quantum transitions, we exploit renormalization-group (RG) and finite-size scaling (FSS) frameworks [20], which constitute the natural theoretical context to effectively describe the behavior of systems in proximity to either a CQT [21,22] or a FOQT [23–25], as well as in a dynamic context [26–28], providing the asymptotic large-size scaling in a variety of situations. Since here we expressly focus on the

* Authors are listed in alphabetic order.

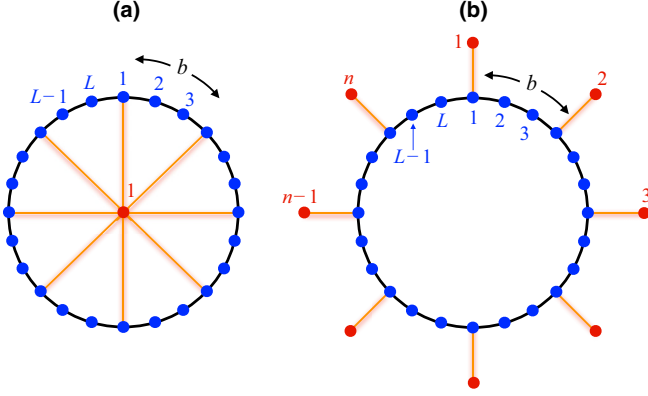


FIG. 1. (a) Sketch of the central-spin model. A ring made of L interacting quantum spins (blue dots) is locally coupled to a single central qubit (red dot) at every b lattice spacings ($b = 3$ in the figure). Note that the typical case studied in the literature is with $b = 1$. (b) Sketch of the sunburst model discussed in this paper. A ring of L spins is locally coupled to n ancillary qubits at every $b = L/n$ lattice spacing ($L = 24$ and $n = 8$ in the figure).

ground-state properties, we make use of the equilibrium FSS formalism [20,21].

We remark that, strictly speaking, decoherence is a dynamic process, while in this paper we are only discussing the equilibrium ground-state properties of the sunburst model. Within our FSS frameworks, this is equivalent to the study of the adiabatic dynamics of a finite-size system, generally characterized by a nonvanishing gap, and thus always possible for sufficiently large timescales, even close to the quantum transitions.

The paper is organized as follows. In Sec. II we introduce the various Hamiltonian terms of the sunburst quantum Ising model, the decoherence functions, and all observables that will be addressed in the subsequent analyses and discuss some simple limit cases. We then study situations where the system parameters are close to the CQT of the Ising ring, in the large-size limit achieved either by keeping fixed the number of ancillary qubits coupled to the ring (Sec. III) or by taking any two consecutive qubits at a fixed distance (Sec. IV). In Sec. V we focus on the regime close to the FOQT line of the Ising ring, while in Sec. VI we discuss the system behavior within the Ising disordered phase. In Sec. VII we summarize our findings and draw conclusions.

II. SUNBURST QUANTUM ISING MODEL

We start by defining our model, where a quantum Ising (\mathcal{I}) spin ring is coupled to a set of ancillary (\mathcal{A}) isolated two-level systems, in a sunburst geometry, as sketched in Fig. 1(b). The quantum Ising chain is a useful theoretical laboratory where fundamental issues of quantum many-body systems can be thoroughly investigated, exploiting the exact knowledge of several features of its phase diagram and quantum correlations. Coupling it to ancillary spins allows us to define a prototypical situation to address the emerging critical behavior of composite quantum many-body systems. This is what we are going to study below.

A. Hamiltonians

Quantum Ising rings are defined by the Hamiltonian

$$\hat{H}_{\mathcal{I}} = - \sum_{x=1}^L (J \hat{\sigma}_x^{(1)} \hat{\sigma}_{x+1}^{(1)} + g \hat{\sigma}_x^{(3)}), \quad (1)$$

where L is the system size, $\hat{\sigma}_x^{(i)}$ are the Pauli matrices on the x th site ($i = 1, 2, 3$ labels the three spatial directions), and $\hat{\sigma}_{L+1}^{(i)} = \hat{\sigma}_1^{(i)}$, corresponding to periodic boundary conditions (PBC). In the following we assume ferromagnetic nearest-neighbor interactions with $J > 0$.

Several results for the low-energy properties of the model (1) have been thoroughly obtained, both in the thermodynamic limit and in the FSS limit with various boundary conditions (see, e.g., Refs. [6,20,29,30] and references therein). Here we recall that the model undergoes a CQT at $g = g_{\mathcal{I}} = J$, belonging to the two-dimensional Ising universality class, separating a disordered phase ($g > g_{\mathcal{I}}$) from an ordered one ($g < g_{\mathcal{I}}$). Approaching the CQT, the system develops long-distance correlations, with a length scale ξ diverging as $\xi \sim |g - g_{\mathcal{I}}|^{-\nu}$, where $\nu = y_g^{-1} = 1$ and y_g is the RG dimension associated with the difference $g - g_{\mathcal{I}}$. The ground-state energy gap $\Delta_{\mathcal{I}}$ (i.e., the energy difference between the two lowest Hamiltonian eigenstates of $\hat{H}_{\mathcal{I}}$) gets suppressed as $\Delta_{\mathcal{I}} \sim \xi^{-z}$, where z is the dynamic critical exponent ($z = 1$). In particular, at the critical point [31],

$$\Delta_{\mathcal{I}}(g_{\mathcal{I}}, L) = \frac{\pi}{2L} + O(L^{-2}). \quad (2)$$

Another independent critical exponent arises from the RG dimension of the symmetry-breaking homogeneous longitudinal field h , coupled to an additional Hamiltonian term of the form $\sum_{x=1}^L \hat{\sigma}_x^{(1)}$, which is $y_h = (2 + d + z - \eta)/2 = 2 - \eta/2$, where d stands for the system dimensionality (here $d = 1$) and $\eta = 1/4$, and thus $y_h = 15/8$ (see, e.g., Refs. [6,20]). Along the $|g/J| < 1$ line, the longitudinal field h drives FOQTs, associated with the avoided level crossing of quantum states with opposite magnetization in finite-size systems, which leads to a discontinuity of the longitudinal magnetization $M = L^{-1} \langle \sum_x \hat{\sigma}_x^{(1)} \rangle$ in the infinite-volume limit. The energy difference of the lowest states along the FOQT line of the Ising ring is exponentially suppressed with increasing L as [32,33]

$$\Delta_{\mathcal{I}}(g < g_{\mathcal{I}}, L) \approx 2 \sqrt{\frac{g_{\mathcal{I}}^2 - g^2}{\pi L}} \left(\frac{g}{J}\right)^L. \quad (3)$$

In our sunburst Ising model, we assume to have n ancillary isolated spin-1/2 systems (qubits), each of them coupled with one spin of the Ising ring, located at an equal distance b from each other, so that $b = L/n$ [see Fig. 1(b)]. We assume they are all described by the same Hamiltonian

$$\hat{H}_{\mathcal{A}} = -\frac{\delta}{2} \sum_{j=1}^n \hat{\Sigma}_j^{(3)}, \quad (4)$$

where $\hat{\Sigma}_j^{(i)}$ are the Pauli matrices of the j th ancillary qubit. The parameter δ quantifies the energy difference between the lowest eigenstates of the Hamiltonian (4), thus providing the energy scale associated with the ancillary system.

The global closed system is formed by two subsystems: the Ising ring with L spins and the n ancillary two-level systems. Their interaction is assumed to be homogeneous for all n qubits and described by the Hamiltonian coupling

$$\hat{H}_{\mathcal{I}\mathcal{A}} = -\kappa \sum_{j=1}^n \hat{\Sigma}_j^{(1)} \hat{\sigma}_{x=jb}^{(1)}, \quad (5)$$

with a strength controlled by the parameter κ .

The full sunburst-Ising-model Hamiltonian

$$\hat{H} = \hat{H}_{\mathcal{I}} + \hat{H}_{\mathcal{A}} + \hat{H}_{\mathcal{I}\mathcal{A}} \quad (6)$$

maintains some of the invariance under translation, i.e., the translation of b lattice spacings. Moreover, the global system has a \mathbb{Z}_2 symmetry, which also involves the ancillary spin operators

$$\begin{aligned} \hat{\sigma}_x^{(1/2)} &\rightarrow -\hat{\sigma}_x^{(1/2)}, & \hat{\Sigma}_j^{(1/2)} &\rightarrow -\hat{\Sigma}_j^{(1/2)}, \\ \hat{\sigma}_x^{(3)} &\rightarrow \hat{\sigma}_x^{(3)}, & \hat{\Sigma}_j^{(3)} &\rightarrow \hat{\Sigma}_j^{(3)}. \end{aligned} \quad (7)$$

Of course, the \mathbb{Z}_2 symmetry associated with the bare Ising chain, i.e.,

$$\hat{\sigma}_x^{(1/2)} \rightarrow -\hat{\sigma}_x^{(1/2)}, \quad \hat{\sigma}_x^{(3)} \rightarrow \hat{\sigma}_x^{(3)}, \quad (8)$$

does not hold anymore. Moreover, one can easily show that the phase diagram and generic global observables are symmetric with respect to changes of the sign of κ and/or δ . Without loss of generality, in the following we restrict ourselves to $\kappa \geq 0$ and $\delta \geq 0$; we also set $J = \hbar = 1$, thus providing the corresponding unities for all the other quantities.

We finally note that, for $n = L$, the above sunburst model may be related to the so-called Heisenberg Ising-Kondo necklace model, for some values of its parameters (see, e.g., Ref. [34]).

B. Decoherence functions and observables

We address the behavior of both subsystems composing the sunburst model (the Ising ring and the ancillary isolated qubits), within the global ground state $|\Psi_0\rangle$. In particular, we aim at studying how their main features, such as the quantum phases and the critical behavior, change when varying the Hamiltonian parameters. To this purpose, we first consider the reduced density matrices associated with the Ising ring ($\rho_{\mathcal{I}}$) and the ancillary subsystem ($\rho_{\mathcal{A}}$) corresponding to the ground state of the global system,

$$\rho_{\mathcal{I}} = \text{Tr}_{\mathcal{A}}[|\Psi_0\rangle\langle\Psi_0|], \quad \rho_{\mathcal{A}} = \text{Tr}_{\mathcal{I}}[|\Psi_0\rangle\langle\Psi_0|], \quad (9)$$

where $\text{Tr}_{\mathcal{A}}[\cdot]$ and $\text{Tr}_{\mathcal{I}}[\cdot]$ denote the partial traces over the respective counterparts. Their coherence properties can be quantified through the purities $P_{\mathcal{I}}$ and $P_{\mathcal{A}}$, defined as

$$P_{\mathcal{I}} = \text{Tr}[\rho_{\mathcal{I}}^2], \quad P_{\mathcal{A}} = \text{Tr}[\rho_{\mathcal{A}}^2], \quad (10)$$

or equivalently by the decoherence factor

$$Q_{\mathcal{I}} = 1 - P_{\mathcal{I}}, \quad Q_{\mathcal{A}} = 1 - P_{\mathcal{A}}. \quad (11)$$

One may also define the corresponding Rényi entanglement entropies $S_{\mathcal{I}}$ and $S_{\mathcal{A}}$ as

$$S_{\mathcal{I}} = -\ln P_{\mathcal{I}}, \quad S_{\mathcal{A}} = -\ln P_{\mathcal{A}}. \quad (12)$$

Exploiting the Schmidt decomposition for bipartitions of pure states [2], one can easily prove that

$$P_{\mathcal{I}} = P_{\mathcal{A}} \equiv P, \quad Q_{\mathcal{I}} = Q_{\mathcal{A}} \equiv Q, \quad S_{\mathcal{I}} = S_{\mathcal{A}} \equiv S. \quad (13)$$

The decoherence factor is limited between $Q = 0$ (corresponding to $P = 1$ and $S = 0$, for a pure reduced state) and $Q \rightarrow 1$ (corresponding to $P \rightarrow 0$, for a completely incoherent many-body state). Now, since Q must be an even function of κ and assuming analyticity at $\kappa = 0$, we may expand it at small κ as

$$Q \approx \frac{1}{2}\kappa^2 \chi_Q + O(\kappa^4), \quad \chi_Q \equiv \left. \frac{\partial^2 Q}{\partial \kappa^2} \right|_{\kappa=0}, \quad (14)$$

where χ_Q keeps the role of decoherence susceptibility.

To characterize the effects of interactions between the two subsystems, we also consider other indicators and observables. As a global quantity, we study the gap Δ , namely, the energy difference between the first excited state and the ground state of the full system. Then we focus on observables related to the Ising ring only, such as correlations of the spin operators $\hat{\sigma}_x^{(1)}$. Due to the \mathbb{Z}_2 symmetry (7), $\text{Tr}[\rho_{\mathcal{I}} \hat{\sigma}_x^{(1)}] = 0$. The two-point correlation function can be written as

$$G(x, y) = \text{Tr}[\rho_{\mathcal{I}} \hat{\sigma}_x^{(1)} \hat{\sigma}_y^{(1)}]. \quad (15)$$

Defining its Fourier-like transform along the ring as

$$\tilde{G}(p) = \frac{1}{L} \sum_{x,y} e^{-ip(x-y)} G(x, y), \quad (16)$$

we consider its zero-momentum component $\chi = \tilde{G}(0)$ and second-moment correlation length.

$$\xi^2 = \frac{1}{4 \sin^2(\pi/L)} \frac{\tilde{G}(0) - \tilde{G}(2\pi/L)}{\tilde{G}(2\pi/L)}, \quad (17)$$

where $2\pi/L$ is the minimum finite momentum along the ring, representing a natural choice of an $O(1/L)$ nonzero momentum for the Ising subsystem. Finally, we also define a Binder-like parameter

$$U = \frac{\text{Tr}[\rho_{\mathcal{I}} \hat{\mu}_2^2]}{(\text{Tr}[\rho_{\mathcal{I}} \hat{\mu}_2])^2} \quad \text{with} \quad \hat{\mu}_2 = \frac{1}{L^2} \sum_{xy} \hat{\sigma}_x^{(1)} \hat{\sigma}_y^{(1)}. \quad (18)$$

C. Extreme cases and notable limits

To understand the role of the Hamiltonian parameters δ and κ describing the ancillary spin system (\mathcal{A}) and the interaction with the Ising ring (\mathcal{I}) [cf. Eqs. (4) and (5)], respectively, it is first useful to discuss some particularly simple cases.

(i) When $\kappa = 0$, the two subsystems \mathcal{A} and \mathcal{I} are trivially decoupled; therefore, $|\Psi_0\rangle = |A_0\rangle_{\mathcal{A}} \otimes |\psi_0\rangle_{\mathcal{I}}$, where $|A_0\rangle_{\mathcal{A}}$ and $|\psi_0\rangle_{\mathcal{I}}$ denote the ground states of the isolated qubits and of the Ising ring.

(ii) When $\delta = 0$, the lowest levels of the global system $\mathcal{A} + \mathcal{I}$ turn out to be twofold degenerate.

(iii) When $\delta \rightarrow \infty$, the state of each of the isolated qubits gets fixed to the eigenstate of $\hat{\Sigma}^{(3)}$ with eigenvalue one, which can also be written as a superposition of the eigenstates $|\pm\rangle$ of $\hat{\Sigma}^{(1)}$. The global ground state is thus again given by the product of states of the two subsystems, i.e., $|\Psi_0\rangle = |A_0\rangle_{\mathcal{A}} \otimes |\psi_0\rangle_{\mathcal{I}}$, where $|A_0\rangle_{\mathcal{A}} = |\phi_0\rangle_1 \otimes \cdots \otimes |\phi_0\rangle_n$,

with $|\phi_0\rangle_j = (|+\rangle_j + |-\rangle_j)/\sqrt{2}$ for the j th ancillary qubit, and $|\psi_0\rangle_{\mathcal{I}}$ is the ground state of the closed Ising ring (note that the interaction term associated with κ vanishes on the ancillary state $|A_0\rangle_{\mathcal{A}}$).

(iv) The $\kappa \rightarrow \infty$ limit is best discussed without fixing $J = 1$, i.e., leaving it free. When $\kappa \rightarrow \infty$, the spins of the Ising rings coupled with the ancillary system are forced to stay in a state described by the reduced density matrix

$$\rho_{\mathcal{A}} = \frac{1}{2} \left(\bigotimes_{j=1}^n |+\rangle_j \langle +| + \bigotimes_{j=1}^n |-\rangle_j \langle -| \right) \quad (19a)$$

in the limit $J \rightarrow \infty$ in the Hamiltonian (1) and

$$\rho_{\mathcal{A}} = \bigotimes_{j=1}^n \frac{1}{2} (|+\rangle_j \langle +| + |-\rangle_j \langle -|) \quad (19b)$$

in the limit $J \rightarrow 0$. As a consequence, the corresponding decoherence measure of the Ising ring ranges from $Q = 1/2$ (for $J \rightarrow \infty$) to $Q = 1 - 1/2^n$ (for $J \rightarrow 0$).

The above considerations hint at the fact that the decoherence effects of the ancillary system may significantly depend on the sunburst-model parameters, as explicitly shown in Fig. 2 (data have been obtained by means of numerical exact diagonalization techniques). Figure 2(a) shows how the decoherence factor Q sets in when the coupling κ between the critical Ising ring and the ancillary qubits increases, keeping the ratio $\delta/\Delta_{\mathcal{I}}$ of their energy scales fixed; here the thermodynamic limit is taken by fixing the number n of qubits in the sunburst geometry (case I below). We observe significant differences when increasing the ring size. Figure 2(b) displays the behavior of the decoherence factor Q , for finite values of δ and κ , as a function of the transverse field strength g (which drives the critical behavior on the Ising ring itself). Here we approach the large-size limit by keeping the distance b between two consecutive ancillary spins fixed and then increasing the chain length L (case II below). We observe the emergence of drastic changes in the decoherence properties of the lattice with g , signaling that different phases are related to qualitative variations of the decoherence factor Q .

In the rest of this paper we want to study the behavior of the sunburst Ising model (6) for generic values of δ and κ , in the limit of large size, by exploiting RG and FSS frameworks. In this respect, we consider two different situations where the large- L limit can be achieved.

(I) We keep the number n of the ancillary spins finite and fixed, while L is increased [same situation as in Fig. 2(a)]. In this case, the bulk properties of the Ising ring are expected to remain unchanged. Thus we expect that, for any value of Hamiltonian parameters κ and δ , the system develops an Ising-like CQT at $g = g_{\mathcal{I}}$ characterized by Ising critical modes along the Ising ring, separating disordered and ordered phases.

(II) We keep the distance $b = L/n$ between two consecutive ancillary spins fixed such that their number increases linearly with L [same as in Fig. 2(b)]. In this case the ancillas are expected to give rise to drastic changes, with transition lines related to the breaking of the global \mathbb{Z}_2 symmetry. In particular, such transitions are expected to move the critical

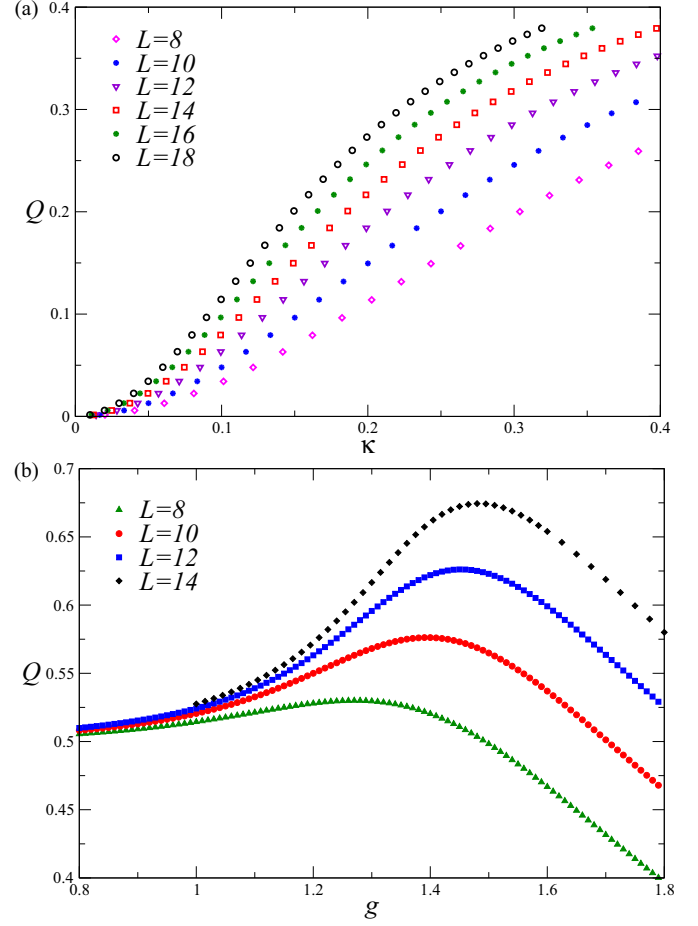


FIG. 2. Behavior of the decoherence factor Q as a function of the various parameters of the sunburst Ising model, for different chain lengths L : (a) Q vs κ for $g = g_{\mathcal{I}} = 1$, $\delta = 2\Delta_{\mathcal{I}}(g_{\mathcal{I}}, L)$, and a fixed number of ancillary spins ($n = 1$) and (b) Q vs g for $\delta = \kappa = 1$, and a fixed distance between two consecutive ancillary spins ($b = 2$).

point $g = g_{\mathcal{I}}$ of the closed Ising ring, generally to $g_c > g_{\mathcal{I}}$, as we will see later.

III. SUNBURST ISING MODEL AT THE CQT, WITH A FINITE NUMBER OF QUBITS

We start by discussing the effects of a finite number n of isolated qubits coupled with the Ising ring, as described by the Hamiltonian (6), which result in the distance between them increasing as $b = L/n$ in the large-size limit (case I above). The ancillary spins play the role of particular defects inserted within the bulk of the Ising system, controlled by the parameter κ [cf. Eq. (5)].

As already mentioned, for an ancillary system with a finite number n of isolated spins, the bulk properties of the Ising ring do not change qualitatively, still showing disordered and ordered phases separated by the CQT at $g = g_{\mathcal{I}} = 1$, independently of the parameters κ and δ . However, some notable change emerges in the FSS behavior close the CQT and of course also in the coherence properties of the Ising ring. In particular, we distinguish between two different FSS regimes: (i) a scaling limit where the interaction with the ancillary

spin-system Hamiltonian acts as a perturbation, and thus both κ and δ are small and scale appropriately with increasing the size of the Ising ring (cf. Sec. III A), and (ii) a FSS limit at fixed values of $\delta > 0$ (cf. Sec. III B).

A. FSS around the closed-Ising-ring criticality

The first question we address is how perturbations arising from the interaction with the ancillary system affect the critical behavior of the closed Ising ring at $g \approx g_{\mathcal{I}}$. When the Hamiltonian $\hat{H}_{\mathcal{I},A}$ [cf. Eq. (5)] acts as a perturbation, we may derive FSS laws using RG arguments based on the scaling behavior of the parameters δ and κ . To address this problem, we should first introduce scaling variables associated with them.

The standard FSS of the closed Ising ring at the CQT is controlled by the scaling variable

$$W = (g - g_{\mathcal{I}})L^{y_g}, \quad y_g = 1. \quad (20)$$

The parameter δ represents the energy scale associated with the isolated qubits. Therefore, its scaling variable should be provided by the ratio between it and the gap $\Delta_{\mathcal{I}}(g_{\mathcal{I}}, L)$ of the Ising ring at criticality, i.e.,

$$A = \frac{\delta}{\Delta_{\mathcal{I}}} \sim \delta L^z, \quad z = 1. \quad (21)$$

To identify the scaling variable associated with the parameter κ , we note that the corresponding perturbations may be interpreted as symmetry-breaking defects for the Ising ring [under the \mathbb{Z}_2 transformation (8) restricted to the Ising-ring subsystem only], controlled by an external operator $\hat{\Sigma}_j^{(1)}$, i.e.,

$$\hat{D}_x = -\kappa \hat{\Sigma}_j^{(1)} \hat{\sigma}_{x=jb}^{(1)}, \quad (22)$$

where the index x denotes the position of the defect along the ring. Since $\hat{\Sigma}_j^{(1)}$ is related to the noncritical ancillary system, we expect it to be not relevant for the determination of the RG dimension of the parameter κ . Therefore, it should be the same as that of the simpler symmetry-breaking defect

$$\hat{D}_x = -\kappa \hat{\sigma}_x^{(1)} \quad (23)$$

for the critical Ising ring, which is equal to $y_{\kappa} = 7/8$ [35]. The scaling variable associated with κ should be thus given by

$$K = \kappa L^{y_{\kappa}}, \quad y_{\kappa} = 7/8. \quad (24)$$

In summary, the FSS limit of all the various observables introduced in Sec. II B can be defined as the large-size limit keeping W , A , and K fixed, therefore for $\delta \sim L^{-z}$ and $\kappa \sim L^{-y_{\kappa}}$.

To monitor the decoherence properties of the Ising ring and the ancillary subsystem, we consider their decoherence factor Q defined in Eqs. (11). A natural ansatz for its scaling behavior in the small- κ and $-\delta$ regime at the CQT of the Ising ring is provided by the scaling equation

$$Q(n, g, \kappa, \delta, L) \approx Q(n, W, K, A). \quad (25)$$

Note that

$$Q(n, W, -K, A) = Q(n, W, K, A) \quad (26)$$

and $Q(n, W, 0, A) = 0$. The scaling in Eq. (25) implies that the corresponding susceptibility χ_Q [cf. Eq. (14)] scales as

$$\chi_Q(n, g, \delta, L) \propto \left(\frac{\partial K}{\partial \kappa} \right)^2 C(n, W, A) = L^{2y_{\kappa}} C(n, W, A). \quad (27)$$

Therefore, the decoherence susceptibility is expected to develop a nonanalytic power-law divergent behavior in the small- δ regime.

We emphasize that the observation of the above FSS laws requires that all Hamiltonian parameters g , δ , and κ must be properly rescaled. In fact, it is easy to verify that the decoherence factor with respect to the parameter κ does not present signatures of data collapse under increasing Ising lattice size L [see Fig. 2(a), where we use the scaling variables $W = 0$ and $A = 2$, but we do not scale κ according to the scaling variable K defined in Eq. (24)]. However, the scaling hypothesis put forward in Eq. (25) is in complete agreement with the data reported in Fig. 3(a), where Q is plotted in terms of the correct scaling variable K . It is also possible to verify that the decoherence susceptibility supports a power-law divergence with L , as outlined in Eq. (27) (see data reported in Fig. 4 for $n = 1$ and 2).

The scaling behavior of the gap of the global system is expected to be

$$\Delta(n, g, \kappa, \delta, L) \approx L^{-z} \mathcal{D}(n, W, K, A). \quad (28)$$

Therefore, the ratio of the global gap with the gap of the closed Ising ring at the QCP is expected to behave as

$$\frac{\Delta(n, g = g_{\mathcal{I}}, \kappa, \delta, L)}{\Delta_{\mathcal{I}}(g_{\mathcal{I}}, L)} \approx \mathcal{D}_c(n, K, A), \quad (29)$$

as shown in Fig. 3(b).

The two-point function (15) should behave analogously, apart from an overall power law, i.e.,

$$G(x, y, n, g, \kappa, \delta, L) \approx L^{-2y_{\varphi}} \mathcal{G}(n, X, Y, W, K, A), \quad (30)$$

where y_{φ} is the RG dimension of the order-parameter operator at Ising transitions, i.e.,

$$y_{\varphi} = (d + z - 2 + \eta)/2 = 1/8, \quad (31)$$

$X = x/L$, and $Y = y/L$ (note that, since the couplings with the ancillary spins break the translation invariance, we must keep the dependence on both spatial variables). In particular, the corresponding susceptibility $\chi = \tilde{G}(0)$ should scale as

$$\chi(n, g, \kappa, \delta, L) \approx L^{1-\eta} \mathcal{B}(n, W, K, A). \quad (32)$$

The RG-invariant quantities (not subject to overall power laws), such as the ratio $R_{\xi} = \xi/L$ and the Binder parameter U [cf. Eqs. (17) and (18)], are expected to behave as (we denote them by R)

$$R(n, g, \kappa, \delta, L) \approx \mathcal{R}(n, W, K, A). \quad (33)$$

Results for the scaling of the RG-invariant ratio

$$\frac{\xi(n, g = g_{\mathcal{I}}, \kappa, \delta, L)}{\xi_{\mathcal{I}}(g = g_{\mathcal{I}}, L)} = \frac{R_{\xi}(n, g = g_{\mathcal{I}}, \kappa, \delta, L)}{R_{\xi}(n, g = g_{\mathcal{I}}, \kappa = 0, \delta, L)}, \quad (34)$$

with $\xi_{\mathcal{I}}$ the correlation length of the standard Ising ring at the QCP, are provided in Fig. 3(c) [note that we prefer to show

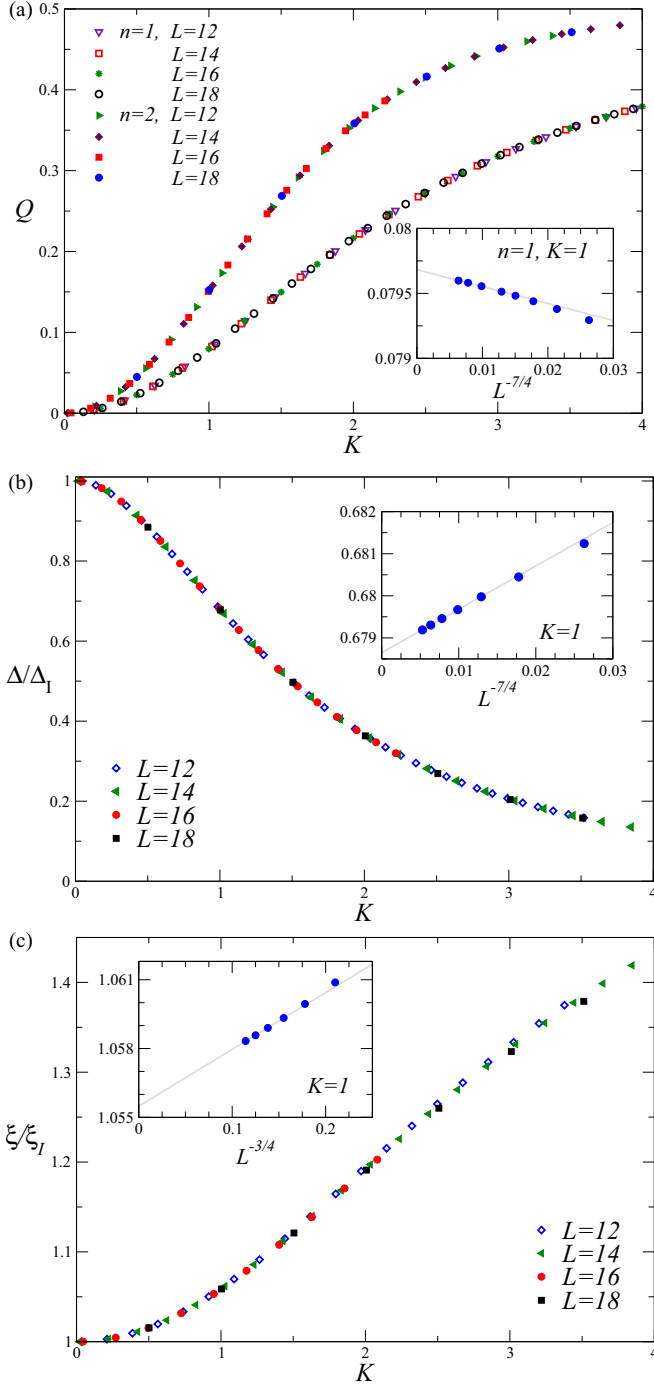


FIG. 3. Scaling of (a) the decoherence factor Q , (b) the ratio of the gaps $\Delta/\Delta_{\mathcal{I}}$ defined in Eq. (29), and (c) the ratio of the correlation lengths $\xi/\xi_{\mathcal{I}}$ defined in Eq. (34), in terms of the variable $K = \kappa L^{7/8}$. The various data sets are for different sizes of the Ising ring and for a fixed number n of isolated qubits. We also fix $W = 0$ and $A = 2$. The predicted scaling behaviors are confirmed, showing convergence to asymptotic large- L FSS curves. The insets display corrections to the scaling of the corresponding quantities at fixed $K = 1$, which are compatible with a decay law $L^{-7/4}$ for Q and $\Delta/\Delta_{\mathcal{I}}$ and with $L^{-3/4}$ for $\xi/\xi_{\mathcal{I}}$ (straight lines interpolate the points for the largest available sizes at our disposal and are drawn to guide to the eye).

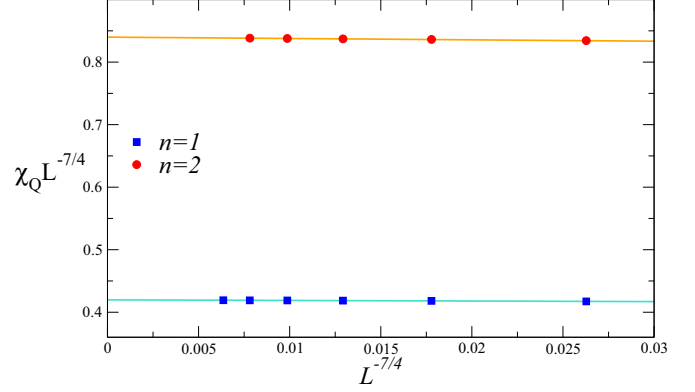


FIG. 4. Rescaled decoherence susceptibility $\chi_Q L^{-7/4}$ versus $L^{-7/4}$ (that is, the way in which scaling corrections are expected to be suppressed) for two values of n and fixed $W = 0$, $A = 1$, and $g = 1$. Systematic errors stemming from the discretization of the second derivative are smaller than the marker sizes. (In the actual computation we use $\kappa = 10^{-4}$ to evaluate χ_Q . Systematic errors are estimated by comparing the discrepancies between data at $\kappa = 10^{-3}$ and 10^{-4} .) Straight lines are drawn to guide the eye. The data confirm the asymptotic power-law divergence $\chi_Q \sim L^{2y_\kappa} = L^{7/4}$ predicted by the scaling (27).

the ratio (34), since it is subject to scaling corrections smaller than $R_\xi = \xi(n, g = g_{\mathcal{I}}, \kappa, \delta, L)/L$.

We point out that the above scaling behaviors are expected to be approached with power-law suppressed corrections, which may depend on the observable considered, analogously to the FSS of closed Ising rings [20,22,35]. The scaling corrections characterizing the approach to the asymptotic FSS are analogous to those of Ising rings in the presence of symmetry-breaking defects discussed in Ref. [35]. We expect that such corrections decay as $L^{-3/4}$ in the case of the ratios $R_\xi = \xi/L$ and $\xi/\xi_{\mathcal{I}}$, since they arise from analytical backgrounds [20,21]. They are instead suppressed as $L^{-7/4}$ in the case of the decoherence factor Q and the gap ratio $\Delta/\Delta_{\mathcal{I}}$. Such $O(L^{-7/4}) = O(L^{-2y_\kappa})$ corrections arise from the nonlinear scaling field [35] associated with the Hamiltonian parameter κ , which is given by $u_\kappa = \kappa + c\kappa^3 + \dots$ (where the quadratic term vanishes, due to the parity-symmetry properties of the Ising ring), and in particular from its third-order term. Plots to highlight the scaling corrections for the observable considered are reported in the insets of Fig. 3 (notice the different dependences on L of the quantities in the x axis, which match the exponent of the various corrections). They are definitely compatible with the expected finite-size power-law suppressions.

Our numerical results also suggest that the dependence on n for a sufficiently large number of ancillary qubits can be taken into account through a redefinition of the scaling variables, after introducing the variable

$$K' = \sqrt{n}K. \quad (35)$$

We provide evidence of this fact in Fig. 5, where the decoherence factor Q is shown versus K' for several values of n

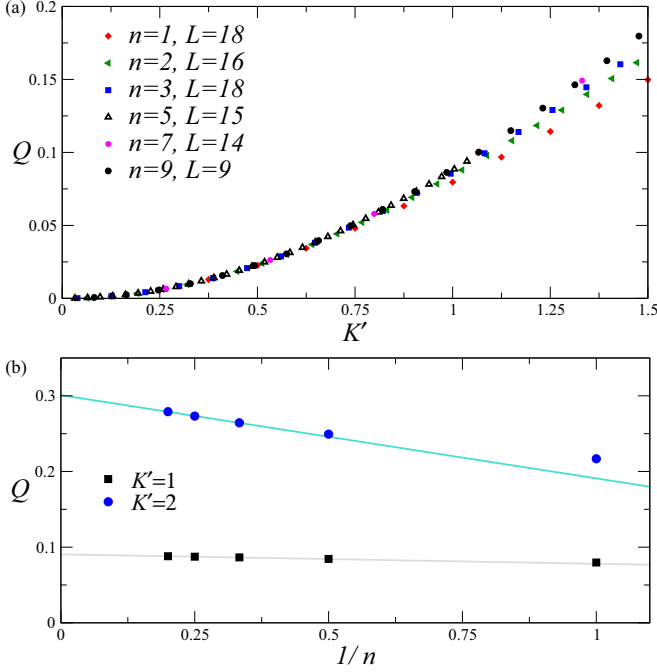


FIG. 5. (a) Decoherence factor Q versus K' at fixed $W = 0$ and $A = 2$ and several values of n . For each n , we only provide data for one of the largest lattice sizes at our disposal. However, we emphasize that scaling corrections are barely visible under the increase of L (cf. Fig. 3). (b) Plot of Q versus $1/n$ for fixed $K' = 1, 2$ at fixed $W = 0$ and $A = 2$. Data are obtained by means of infinite-volume extrapolations ($L \rightarrow \infty$ at fixed n), assuming $L^{-7/4}$ scaling corrections. Straight lines are drawn to guide the eye. Extrapolations up to $n = 5$ are compatible with a $1/n$ approach. The data provide a robust check of the scaling behavior reported in Eq. (36).

[Fig. 5(a)]. The plot supports the scaling behavior

$$Q(n, g, \kappa, \delta, L) \approx \tilde{Q}(W, K', A), \quad (36)$$

with corrections that are apparently suppressed as $1/n$, as shown in Fig. 5(b). Analogous behaviors are observed for the other quantities. Note that the square-root power of n in Eq. (35) is probably related to the fact that it actually takes into account the effect of n independent ancillary systems.

The above scaling behaviors show that the low-energy critical behavior of the Ising ring experiences rapid and drastic changes under the effects of perturbations arising from interactions with the ancillary qubits, even in the case of one single ancillary isolated qubit.

B. Behavior at finite ancillary energy scale δ

As already mentioned, in the case of a finite number of ancillary spins, the system remains critical at $g = g_{\mathcal{I}}$, even for finite values of the energy scale δ and the interaction parameter κ . The FSS behavior changes, similarly to changes arising from variations of boundary conditions in closed critical systems. However, the variations for finite κ and δ appear smooth, i.e., much smoother than the drastic and rapid changes arising from their turning on at small κ and δ (see Sec. III A).

In the following we consider the FSS limit, keeping the Hamiltonian parameter $\delta > 0$ fixed. The numerical results at

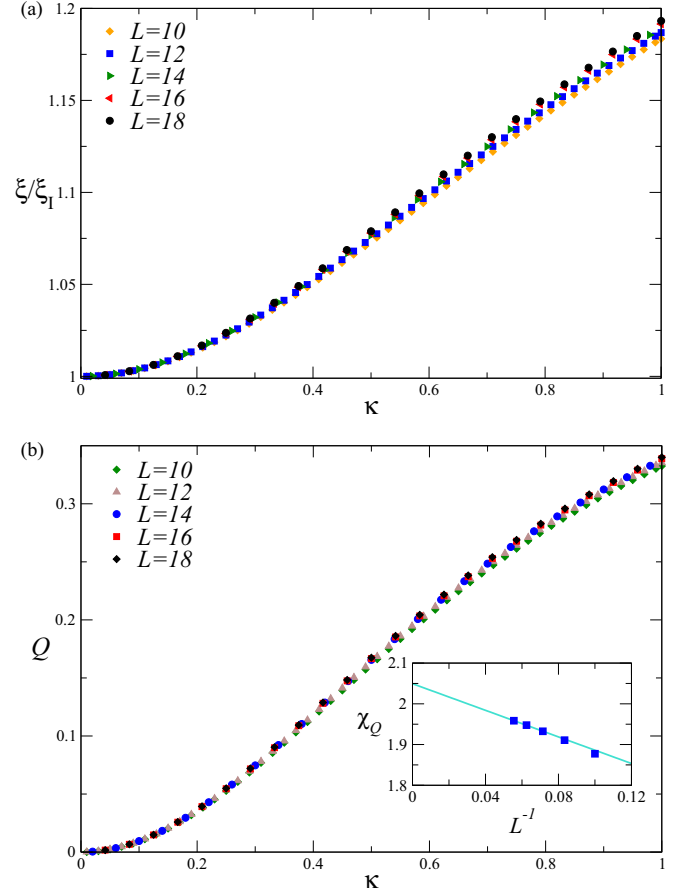


FIG. 6. (a) Ratio $\xi/\xi_{\mathcal{I}}$ and (b) decoherence factor Q versus κ , for finite $n = 1$, $\delta = 1$, and $g = g_{\mathcal{I}} = 1$. The data show a smooth behavior with κ , without any significant dependence on the size of the Ising ring, suggesting that the effect at the QCP remains essentially local when $\delta > 0$ is kept finite in the large- L limit. The inset in (b) shows that the decoherence susceptibility χ_Q converges to a constant as L^{-1} in the large-volume limit.

$g = g_{\mathcal{I}}$ show that the observables remain critical, but their FSS curves change when varying κ and δ , without apparent nonanalyticities, like those observed around $\kappa = \delta = 0$ [Fig. 6(a)]. It is also worth noting that, when keeping $\delta > 0$ fixed, the decoherence factor Q is expected to behave smoothly around $\kappa = 0$; thus its susceptibility χ_Q is not expected to diverge in the large- L limit, unlike around $\delta = 0$. This is confirmed by the results in Fig. 6(b), where the smooth behavior of the decoherence Q and its susceptibility χ_Q completely agrees with the presented scenario.

IV. SUNBURST ISING MODEL AT THE CQT, WITH QUBITS AT FIXED DISTANCE

We now discuss a different situation, where the isolated qubits of the ancillary system become infinite and their contacts with the Ising ring are maintained at a fixed distance b (case II in Sec. II C). Therefore, in the large-size limit, $L \rightarrow \infty$ and also $n = L/b \rightarrow \infty$. Again we distinguish between two regimes: (i) The interaction with the ancillary qubits represents a small perturbation, in which case we describe the

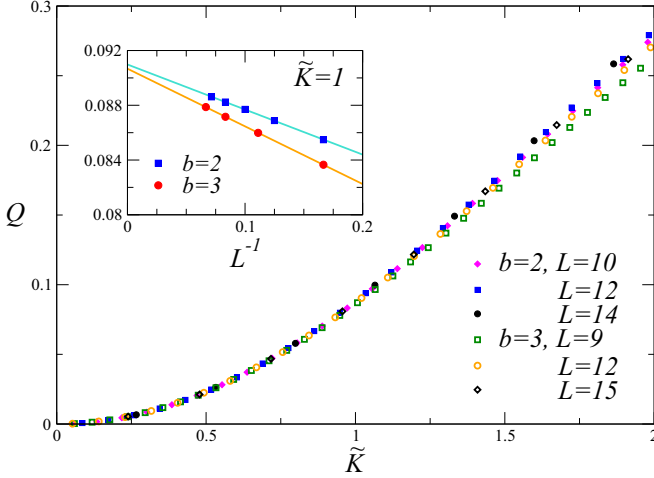


FIG. 7. Scaling of the decoherence factor Q versus \tilde{K} for fixed $W = 0$, $A = 2$, and $b = 2, 3$. In the inset, large-volume extrapolations for $b = 2$ and $b = 3$ are consistent with a decay L^{-1} and are compatible with each other. These data definitely support the scaling behavior of Eq. (38), thus implying the power-law divergence of the corresponding decoherence susceptibility: $\chi_Q \sim L^{2\tilde{y}_\kappa}$ with $2\tilde{y}_\kappa = 11/4$ [see Eq. (39)]. They also show that the parameter b does not play a major role, apart from entering the definition of \tilde{K} .

distortion of the FSS behavior around the quantum transition of the Ising ring (cf. Sec. IV A), and (ii) the effect of the interaction with the ancillary qubits is substantial, in which case we show how the phase diagram gets changed, still developing an Ising-like transition at $g_c > g_{\mathcal{I}}$ (cf. Sec. IV B).

A. FSS around the closed-Ising-ring criticality

As done in Sec. III A, in order to discuss the effects of the perturbations arising from the ancillary spin system at the CQT of the Ising ring, we should first determine the corresponding scaling variables. For this purpose, we make reasonable guesses based on the results for a finite number of ancillary spins and in particular for a large number of n . Our working hypothesis is that A , defined in Eq. (21), still remains a good scaling variable (essentially because δ is again the gap of the ancillary spin system), but we need to change K [cf. Eq. (24)]. Indeed, using Eq. (35) and noting that $n = L/b$ in the case at hand, we arrive at the following expression:

$$\tilde{K} = \kappa b^{-1/2} L^{\tilde{y}_\kappa}, \quad \tilde{y}_\kappa = y_\kappa + 1/2 = 11/8. \quad (37)$$

Therefore, the decoherence properties around the Ising-ring criticality are expected to obey the scaling behavior

$$Q(b, g, \kappa, \delta, L) \approx \tilde{Q}(W, \tilde{K}, A). \quad (38)$$

This implies that

$$\chi_Q(b, g, \delta, L) \approx L^{2\tilde{y}_\kappa} \tilde{\mathcal{C}}(W, A), \quad (39)$$

showing a faster divergence with respect to that for a finite number of ancillary spins [compare with Eq. (27)]. Numerical data for the decoherence factor Q reported in Fig. 7 fully support this scaling ansatz, within scaling corrections that, for fixed b , appear to be suppressed as L^{-1} . Analogous behaviors

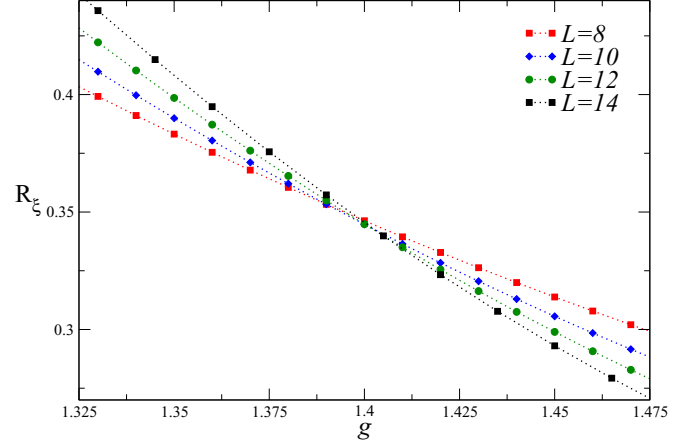


FIG. 8. The RG-invariant quantity R_ξ versus g for $b = 2$ and finite $\delta = \kappa = 1$. The crossing point $g_c(\kappa = 1, \delta = 1) \approx 1.40$ signals the Ising-like transition between the paramagnetic and the ordered phase of the lattice model, which moves away from the Ising critical point $g_{\mathcal{I}} = 1$.

are developed by the other observables (not shown), for example, in the case of RG-invariant quantities

$$R(b, g, \kappa, \delta, L) \approx \tilde{\mathcal{R}}(W, \tilde{K}, A). \quad (40)$$

We also expect that the microscopic distance b between the ancillary contacts does not play a major role, apart from entering the definition of the scaling variable \tilde{K} .

B. Phase diagram for finite κ and δ

For finite values of the Hamiltonian parameters κ and δ , the ancillary system may give rise to a modification of the phase diagram. In particular, we expect that the system at $g = g_{\mathcal{I}}$ does not remain *critical*. Since the whole system has a global \mathbb{Z}_2 symmetry, we may still have Ising-like transitions, but their positions could shift to other values of g . This is clearly demonstrated by the numerical results shown in Fig. 8, which provide evidence of a transition along a surface at $g_c(\kappa, \delta) > g_{\mathcal{I}}$ (see Sec. VI for further details).

To address the nature of the transition, assuming that R_ξ is a monotonic function of g , one can invert Eq. (33) and substitute it into the Binder dependence such that in the large-volume limit

$$U(b, L, g, \delta, \kappa) \approx \mathcal{U}_{\mathcal{I}}(R_\xi). \quad (41)$$

This relation is particularly useful to compare the universality class of different models, as the function $\mathcal{U}_{\mathcal{I}}$ only depends on the boundary conditions and the universality class at the transition. Moreover, it does not require the tuning of any nonuniversal parameter to be satisfied, so the universality class of two different lattice models can be easily compared. Leading scaling corrections to this formula are expected to get suppressed as $L^{-3/4}$ [20,21]. In Fig. 9 we show results for the Binder parameter U vs the RG-invariant quantity $R_\xi = \xi/L$ [cf. Eqs. (18) and (17), respectively] at finite values of δ and κ , together with the interpolation of the universal Ising curve $\mathcal{U}_{\mathcal{I}}(R_\xi)$ for PBC.

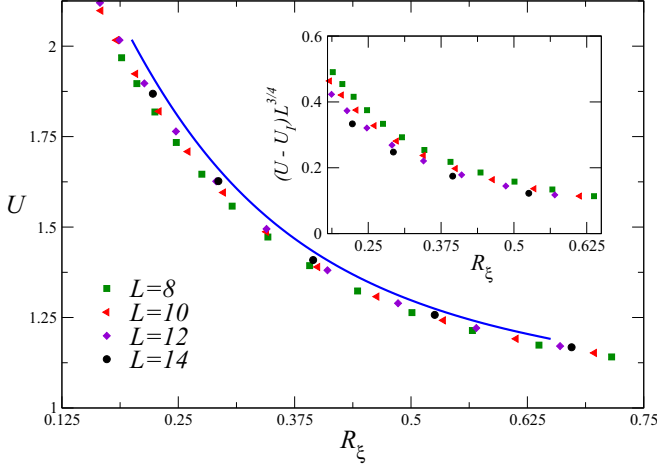


FIG. 9. Binder parameter U versus the RG-invariant ratio R_ξ for $b = 2$, $\delta = 1$, and $\kappa = 1$. The blue line represents the infinite-volume extrapolation of the universal curve $\mathcal{U}_T(R_\xi)$ for the conventional Ising ring. Data for finite δ and $\kappa > 0$ approach the same RG universal curve of the Ising universality class with PBC. In the inset, we show $(U - U_\infty)L^{3/4}$ in terms of R_ξ . The behavior of the scaling corrections appear substantially consistent with their expected $O(L^{-3/4})$ asymptotic suppression.

To better understand the features of the phase diagram in the (g, κ) plane, we keep $\delta > 0$ fixed and discuss the behavior when varying κ around $\kappa = 0$, around the pure Ising-ring QCP ($g = g_{\mathcal{I}}$). Note that this is different from the case considered in Sec. IV A, where δ was rescaled as $\delta \sim L^{-z}$. Therefore, the scaling behaviors outlined in Sec. IV A are not expected to hold anymore.

To describe how the QCP moves, we may analyze the behavior of the scaling field u_g under the effect of κ . While in the previous analyses we considered $u_g = g - g_{\mathcal{I}}$ [cf. Eq. (20)], here we should take into account the presence of the interaction with the ancillary system and therefore its dependence on κ . Since the global system is invariant when changing the sign of κ , u_g must be an even function of κ . The additional requirement of analyticity with respect to the Hamiltonian parameters then gives

$$u_g \approx g - g_{\mathcal{I}} - C_\kappa(\delta, b)\kappa^2. \quad (42)$$

Note that no terms containing only δ must be present, since we must recover the closed Ising-ring expression when $\kappa = 0$ for any $\delta > 0$.

The critical point occurs when $u_g = 0$; thus we expect

$$g_c(\kappa) \approx g_{\mathcal{I}} + C_\kappa(\delta, b)\kappa^2, \quad (43)$$

which should hold for sufficiently small values of κ . This behavior has been numerically checked by estimating the critical points $g_c(\kappa)$ for various values of κ (see Fig. 10).

Therefore, assuming Ising transitions related to the breaking of the global \mathbb{Z}_2 symmetry, we expect to observe a scaling behavior around g_c in terms of the scaling variable

$$\tilde{W} = (g - g_c)L^{y_g}, \quad y_g = 1. \quad (44)$$

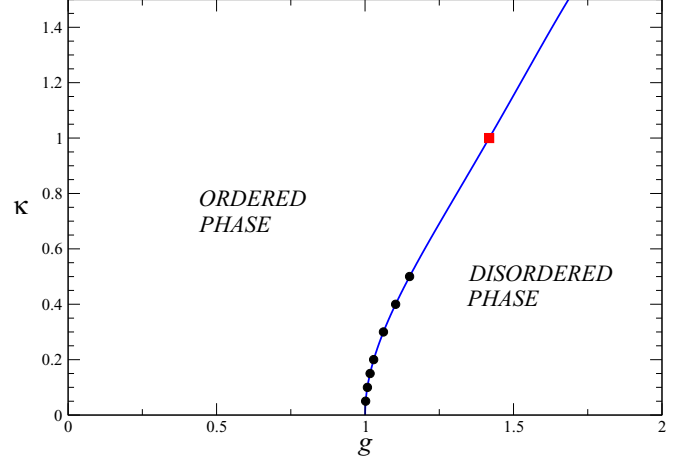


FIG. 10. Sketch of the g - κ phase diagram of the sunburst quantum Ising model with $b = 2$ at $\delta = 1$. The red square at $\kappa = 1$ corresponds to the specific case analyzed in Fig. 8, while the black circles have been obtained by analyzing the RG-invariant quantity ξ/ξ_I [cf. Eq. (34)] up to $L = 12$. The estimates of the critical points are fully consistent with the behavior reported in Eq. (43), i.e., $g_c(\kappa) - g_{\mathcal{I}} \sim \kappa^2$ for sufficiently small values of κ .

This also implies, at $g = g_{\mathcal{I}}$ and for small κ , the scaling behavior (keeping $\delta > 0$ fixed)

$$Q(g = g_{\mathcal{I}}, b, \kappa, \delta, L) \approx Q_s(\delta, W_s), \quad (45)$$

$$R(g = g_{\mathcal{I}}, b, \kappa, \delta, L) \approx R_s(\delta, W_s), \quad (46)$$

where

$$W_s = \kappa^2 L \sim \tilde{W}(g = g_{\mathcal{I}}). \quad (47)$$

The above continuous transition line separates the phase diagram in ordered and disordered phases for $g < g_c$ and $g > g_c$, respectively. Results inherent to the presented FSS ansatz are shown in Fig. 11, where the decoherence factor Q nicely scales in terms of $b^{-1}W_s$. This plot also supports the fact that the coefficient C_κ of the κ^2 term in Eq. (43) behaves as $C_\kappa \approx b^{-1}f(\delta)$, implying again that the microscopic distance b does not play a major role, apart from entering the redefinition of the scaling variable W_s .

On the basis of the above results, in Fig. 10 we provide a sketch of the phase diagram of the sunburst Ising model with $b = 2$, at $\delta = 1$, in the space of parameters g and κ . An analogous scenario is expected to hold for any $\delta > 0$ and any value of $b \geq 1$.

V. BEHAVIOR ALONG THE FOQT LINE OF THE ISING RING

We now discuss the effects of the interaction with the ancillary system at the FOQT line of the Ising ring, i.e., when $g < g_{\mathcal{I}}$, and small values of κ and δ , around $\kappa = \delta = 0$. Again we address the problem within a FSS framework, which recently has been developed also at FOQTs (see, e.g., Refs. [20,23]). We consider the interaction with the ancillary system as a perturbation, in particular when also its energy scale δ is small. We recall that, at a FOQT, the gap $\Delta_{\mathcal{I}}(g, L)$ is generally exponentially suppressed in the case of neutral

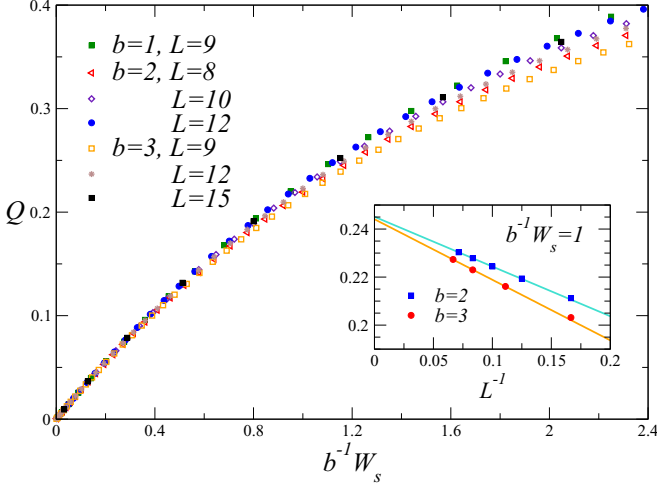


FIG. 11. Plot of Q versus $b^{-1}W_s$ for finite $g = g_T$ and $\delta = 2$ and various values of b . The data nicely confirm the FSS (45). In the inset, scaling corrections at $b^{-1}W_s = 1$ are compatible with an L^{-1} behavior. Note that the large-volume extrapolations for the two shown values of $b = 2$ and $b = 3$ are compatible with each other. The straight lines are drawn to guide the eye.

boundary conditions [23,24], such as for Ising rings [cf. Eq. (3)].

A. Case of a finite number of ancillary spins

We follow the same ideas at the basis of the FSS description of FOQTs of Ising systems driven by an external magnetic field (see, in particular, Ref. [20]). We introduce the

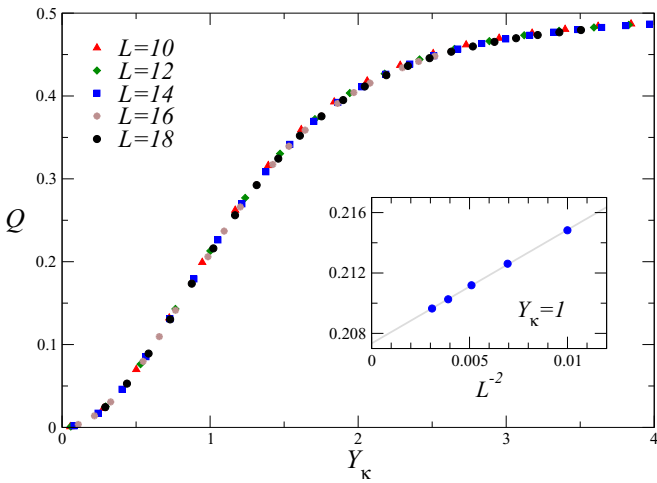


FIG. 12. Scaling of the decoherence factor Q versus Y_κ at a FOQT with $n = 2$, $g = 0.9$, and $Y_\delta = 2$. Data nicely collapse with increasing lattice size, supporting the presented FSS theory [see, in particular, Eq. (49)]. In the inset, scaling corrections at $Y_\kappa = 1$ are in complete agreement with an L^{-2} decay. The straight line is drawn to guide the eye.

scaling variables

$$Y_\kappa = \frac{\kappa}{\Delta_{\mathcal{I}}(g, L)}, \quad Y_\delta = \frac{\delta}{\Delta_{\mathcal{I}}(g, L)}. \quad (48)$$

Here Y_κ is proportional to the ratio of the energy change arising from the perturbation associated with κ and the exponentially suppressed gap of the pure Ising ring [23], while Y_δ is the ratio between the gap of the unperturbed ancillary system and that of the Ising ring. Therefore, we consider a FSS limit keeping the scaling variables Y_κ and Y_δ fixed. The decoherence factor defined in Eq. (11) is expected to behave as

$$Q(n, g, \kappa, \delta, L) \approx Q(n, Y_\kappa, Y_\delta). \quad (49)$$

Numerical results for the scaling of Q in Fig. 12 fully support the presented FSS hypothesis. Note that this also implies

$$\chi_Q(n, g, \delta, L) \approx \Delta_{\mathcal{I}}(g, L)^{-2} \mathcal{C}(n, Y_\delta). \quad (50)$$

In turn this implies that, since $\Delta_{\mathcal{I}}(g, L)$ is exponentially suppressed [cf. Eq. (3)], the coherence shows an exponentially rapid drop around $\kappa = 0$. Like the behavior at the CQT, we again observe that the dependence on n can be absorbed within the scaling variables for sufficiently large n , by replacing Y_κ with

$$Y'_\kappa = \sqrt{n} Y_\kappa. \quad (51)$$

This clearly emerges from the plot in Fig. 13, where the decoherence factor Q is shown as a function of Y'_κ at fixed Y_δ for several values of n . The analysis follows the same reasoning as that carried out in the case of CQTs (see Fig. 5). Indeed, the data are consistent with an asymptotic scaling behavior

$$Q(n, g, \kappa, \delta, L) \approx Q(Y'_\kappa, Y_\delta) \quad (52)$$

in the FSS limit, keeping Y'_κ fixed.

Analogously to the behavior observed at the CQT, the above scaling behavior changes significantly when $\delta > 0$ is kept fixed in the large-size limit. In this case, the decoherence factor appears to depend smoothly on κ , even at $\kappa = 0$. Therefore, also the corresponding susceptibility χ_Q does not diverge in the large-size limit. Results are shown in Fig. 14 for $\delta = 1$.

B. Case of ancillary spins at fixed distance

We now discuss the behavior at the FOQT of the Ising ring when the ancillary spins are located at fixed distance b , which results in their number scaling as $n = L/b$. Similarly to the CQT case, on the basis of the large- n scaling variable Y'_κ introduced in Eq. (51), we argue that the appropriate scaling variable when $n = L/b$ is simply obtained by replacing n with L/b , thus obtaining

$$\tilde{Y}_\kappa = \frac{kL^{1/2}}{b^{1/2} \Delta_{\mathcal{I}}(g, L)}. \quad (53)$$

The other scaling variable Y_δ should be appropriate also in this case. Therefore, the decoherence factor is expected to scale as

$$Q(b, g, \kappa, \delta, L) \approx \tilde{Q}(\tilde{Y}_\kappa, Y_\delta). \quad (54)$$

Numerical results displayed in Fig. 15 provide evidence of this scaling behavior, within corrections that appear to decay as L^{-1} .

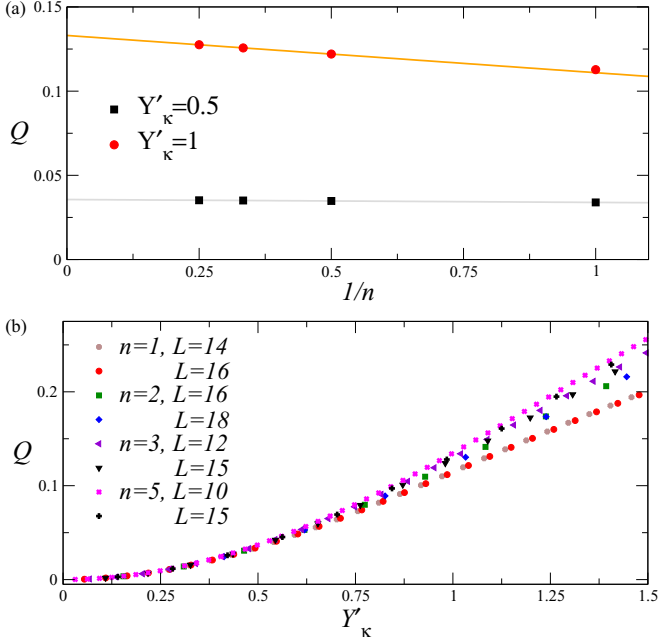


FIG. 13. (a) Decoherence factor Q versus the inverse number of ancillary spins $1/n$ for fixed $Y'_\kappa = 0.5$ and 1 . For each value of n , the infinite-volume extrapolations for the decoherence are computed assuming L^{-2} scaling corrections. (b) Decoherence factor Q versus Y'_κ for many n and $Y_\delta = 2$ at a FOQT ($g = 0.9$). Data collapse improves along the whole curve with an increasing number of ancillary spins. These plots clearly support the scaling (52), when n is increased. Indeed, the data appear to approach a scaling curve in the large- n limit, which is clearly distinct from the curve for $n = 1$, at least for sufficiently large values of Y'_κ .

VI. BEHAVIOR IN THE DISORDERED PHASE

We finally discuss the effects of the interaction with the ancillary system within the disordered phase of the Ising ring. In this case we expect a trivial behavior when keeping n fixed, i.e., a substantial independence of the size L when increasing it, and a smooth behavior as a function of κ and δ . However, it is interesting to note that, when increasing n , the \sqrt{n} law emerges also within the disordered phase. Indeed, the behavior is generally characterized by a dependence on $\sqrt{n}\kappa$ for sufficiently large n , and therefore on $\kappa L^{1/2}b^{-1/2}$ when we consider ancillary spins at fixed distance. In Fig. 16 numerical results for $b = 2$ and 3 support this hypothesis.

According to previous sections, a reasonable doubt might arise regarding the probed phase of the lattice model, as the continuous transition line moves to higher values $g_c > g_I$ when b is fixed (cf. Fig. 10). However note that, with increasing the lattice size, we also need to rescale $\kappa \sim L^{-1/2}$ to keep $\kappa L^{1/2}b^{-1/2}$ fixed. Thus, in the thermodynamic limit, we only explore the phase diagram in the neighborhood of $\kappa = 0$, where the system is always disordered for any $g > g_I$.

VII. SUMMARY

We have investigated the ground-state properties of a system of quantum spin-1/2 chains arranged in a sunburstlike

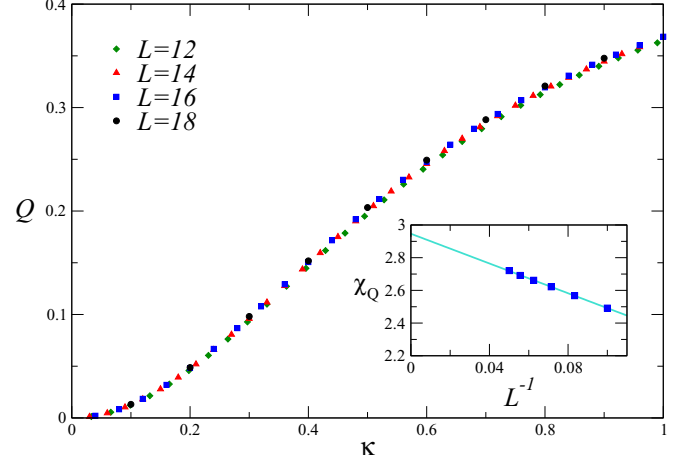


FIG. 14. Decoherence factor Q versus κ for finite $g = 0.9$ and $\delta = 1$, with a single ancillary spin. The plot shows that Q behaves as a smooth function of κ , as well as its susceptibility χ_Q , which converges to a constant as L^{-1} , in the large-volume limit (see the inset, where the line is drawn to guide the eye).

geometry, as sketched in Fig. 1(b), where the L spins in the ring are supposed to be described by a one-dimensional quantum Ising model (1). The latter represents a prototypical quantum many-body system showing different quantum phases, separated by FOQTs and a CQT, when varying the intensity of the external transverse and longitudinal fields. Although the full system is considered to be isolated and thus governed by a unitary evolution, its subparts (namely, the Ising ring and the external ancillary isolated spins) are naturally subject to decoherence, as revealed by the decoherence factor Q [Eq. (11)] and its susceptibility χ_Q [Eq. (14)].

In this exploratory study of the sunburst Ising model, we addressed the properties of its subsystems within the ground

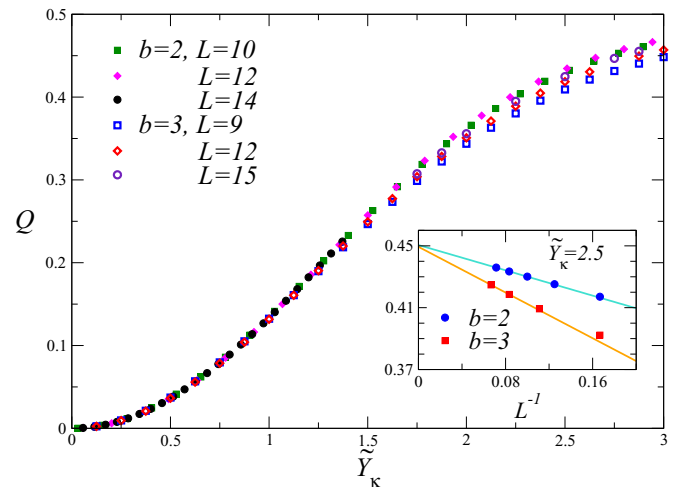


FIG. 15. Decoherence factor Q versus \tilde{Y}_κ for $Y_\delta = 2$ and $b = 2$ and 3 , at a FOQT ($g = 0.9$). Data nicely collapse with increasing lattice size, in agreement with the scaling behavior reported in Eq. (54). In the inset, scaling corrections at fixed $\tilde{Y}_\kappa = 2.5$ appear to decay as L^{-1} .

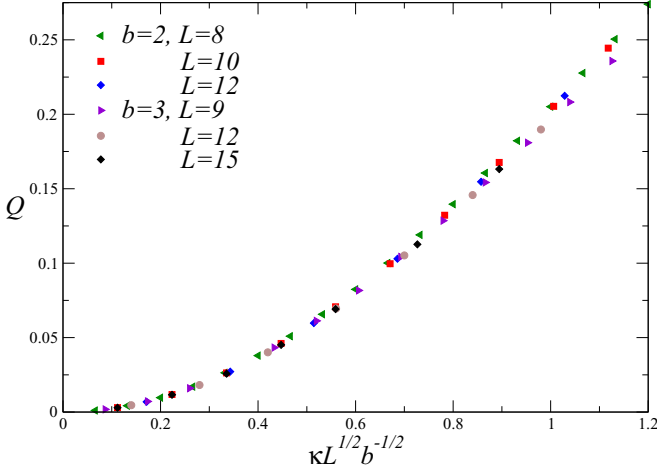


FIG. 16. Decoherence function Q versus $\kappa L^{1/2}b^{-1/2} = \kappa\sqrt{n}$ at the disordered phase, with $g = 1.5$ and $\delta = 1$. These data clearly support the \sqrt{n} law of the dependence of the observables in the large- n limit and in particular of the decoherence factor.

state of the global system, under different conditions controlled by the various Hamiltonian parameters, such as the Ising transverse field g , the energy scale δ of the ancillary system, and the interaction strength κ between the two subsystems. Even though we discussed the behavior in the large-size limit, we essentially considered finite-size systems exploiting FSS frameworks, and thus the equilibrium ground-state properties could be associated with the adiabatic dynamics. Finite-size systems generally have a nonvanishing gap; therefore, it is always possible to conceive adiabatic evolutions for sufficiently large timescales, even close to the quantum transitions.

Substantially different regimes emerge. At small κ they are related to the different phases of the Ising ring. We observed rapid changes with respect to variations of the Hamiltonian parameters close to quantum transitions, such as along the FOQT line ($|g| < g_{\mathcal{I}}$) and at the CQT ($g \simeq g_{\mathcal{I}}$) of the Ising ring, with the emergence of peculiar scaling regimes. To perform this analysis we exploited RG and FSS frameworks [20], which allowed us to effectively describe the behavior of systems in proximity to either CQTs or FOQTs. We distinguished two notable large- L limits where FSS laws develop: (i) the case in which the number n of isolated spins of the ancillary system is kept fixed and (ii) the case in which their number increases as $n = L/b$, being located at fixed spatial intervals of size b , to maintain a residual translation invariance. In the following we summarize the main results.

For sufficiently small values of the Hamiltonian parameters δ and κ , the decoherence factor and also the correlations along the Ising ring show nonanalytic behaviors at the CQT, controlled by scaling variables associated with the Hamiltonian parameters κ and δ . The one associated with the interaction strength κ is given by (i) $K = \kappa L^{y_{\kappa}}$, where $y_{\kappa} = 7/8$, for a finite number of ancillary spins (the RG exponent y_{κ} is related to that of the symmetry-breaking defects [35]), and (ii) $\tilde{K} = \kappa L^{\tilde{y}_{\kappa}}$, with $\tilde{y}_{\kappa} = y_{\kappa} + 1/2 = 11/8$, for an infinite number of ancillary spins. The crossover between the two

regimes is essentially controlled by the peculiar \sqrt{n} dependence when increasing n , which can be reabsorbed by an appropriate redefinition of the scaling variable associated with the Hamiltonian parameter κ , i.e., $K' = \sqrt{n}K$. Therefore, the scaling variable \tilde{K} reflects the fact that the large- n behavior is essentially controlled by the scaling variable $\sqrt{n}K$ leading to \tilde{K} when replacing $n = L/b$. The scaling variable associated with the ancillary energy scale δ turns out to be $A = \delta L^z$, with $z = 1$, in both cases (i) and (ii). The scaling behavior of the decoherence factor, reported in Eqs. (25) and (38), implies rapid changes when moving κ and δ from zero, due to the divergence of the corresponding susceptibility [cf. Eq. (14)], as (i) $\chi_Q \sim L^{2y_{\kappa}}$ for finite n and (ii) $\chi_Q \sim L^{2\tilde{y}_{\kappa}}$ for $n = L/b$ (keeping A fixed).

The impact on the decoherence behavior in the small- κ and $-\delta$ regimes appears even more drastic at the FOQT transition line, where the gap $\Delta_{\mathcal{I}}$ of the pure Ising ring gets suppressed exponentially when increasing L . The scaling variables turn out to be (i) $Y_{\kappa} = \kappa/\Delta_{\mathcal{I}}$ for finite n and (ii) $\tilde{Y}_{\kappa} = \kappa L^{1/2}/b^{1/2}\Delta_{\mathcal{I}}$ for $n = L/b$, while $Y_{\delta} = \delta/\Delta_{\mathcal{I}}$ in both cases (i) and (ii). As a consequence, the decoherence susceptibility now diverges exponentially, i.e., $\chi_Q \sim \Delta_{\mathcal{I}}^{-2} \sim e^{cL}$.

The above behaviors change when considering the large-size limit while keeping the energy scale $\delta > 0$ of the ancillary subsystem fixed. In particular, we observed a smooth dependence of the various quantities on κ even around $\kappa = 0$, when the number n of ancillary spins is finite. However, this is effectively controlled by the product $\sqrt{n}\kappa$ when n increases and by $\kappa L^{1/2}$ when n increases linearly as $n = L/b$. This led to the predictions that the decoherence susceptibility remains finite [$\chi_Q = O(1)$] at finite n , while it increases as $\chi_Q \sim L$ for $n \sim L$. Likewise, we observed an analogous behavior of χ_Q with L , at the disordered phase of the Ising ring (i.e., when $g > g_{\mathcal{I}}$).

Finally, we have analyzed the global phase diagram of the model in the space of the Hamiltonian parameters g , κ , and δ . As expected from considerations based on the global symmetry of the system, which maintains a \mathbb{Z}_2 symmetry [cf. Eq. (7)], there is a line of Ising-like CQTs separating disordered and ordered phases. This line runs for $g_c(\kappa, \delta) > g_{\mathcal{I}}$, and in particular close to $\kappa = 0$ it behaves as $g_c(\kappa, \delta) \approx g_{\mathcal{I}} + C_{\kappa}\kappa^2$. Around it, the decoherence factor behaves (i) as a smooth function of κ for finite n or (ii) as $\kappa L^{1/2}$ for $n = L/b$.

Our analysis has focused on the sunburst Ising model with a one-dimensional geometry (namely, the subsystem made of L interacting spins is effectively a ring). However, from a conceptual point of view, it is straightforward to generalize such model to higher dimensions (for example, the two-dimensional case corresponds to an interacting spin system on a square lattice, where some spins are coupled with isolated qubits, following a regular pattern). Unfortunately, the lack of integrability of such a model drastically limits the possibilities of standard numerical approaches up to very small sizes.

It would be tempting to also investigate the sunburst model under dynamic out-of-equilibrium protocols for examples arising from sudden quenches of one-Hamiltonian parameter, such as those already considered within the more familiar central spin models (see, e.g., Ref. [20]). In this context, one could study peculiar mechanisms arising in composite

quantum systems, such as the onset of decoherence in time or the exchange of heat and work between the various subportions of the whole system, characterizing their quantum thermodynamic properties.

We point out that all the results obtained in this paper have been carefully checked by means of numerical simula-

tions for systems with a limited number of coupled qubits ($L \lesssim 20$). This suggests the possibility to devise near-term experiments with quantum simulators to access our predictions directly in the laboratory, e.g., by means of trapped ions [36,37], ultracold atoms [38,39], or superconducting qubits [40,41].

-
- [1] W. H. Zurek, Decoherence, einselection, and the quantum origins of the classical, *Rev. Mod. Phys.* **75**, 715 (2003).
- [2] M. A. Nielsen and I. L. Chuang, *Quantum Computation and Quantum Information* (Cambridge University Press, Cambridge, 2010).
- [3] N. Lambert, Y.-N. Chen, Y.-C. Cheng, C.-M. Li, G.-Y. Chen, and F. Nori, Quantum biology, *Nat. Phys.* **9**, 10 (2013).
- [4] F. Campaioli, F. A. Pollock, and S. Vinjanampathy, in *Thermodynamics in the Quantum Regime*, edited by F. Binder, L. A. Correa, C. Gogolin, J. Anders, and G. Adesso (Springer, Berlin, 2018), pp. 207–225.
- [5] G. Benenti, G. Casati, K. Saito, and R. S. Whitney, Fundamental aspects of steady-state conversion of heat to work at the nanoscale, *Phys. Rep.* **694**, 1 (2017).
- [6] S. Sachdev, *Quantum Phase Transitions* (Cambridge University Press, Cambridge, 1999).
- [7] W. H. Zurek, Environment-induced superselection rules, *Phys. Rev. D* **26**, 1862 (1982).
- [8] F. M. Cucchietti, J. P. Paz, and W. H. Zurek, Decoherence from spin environments, *Phys. Rev. A* **72**, 052113 (2005).
- [9] H. T. Quan, Z. Song, X. F. Liu, P. Zanardi, and C. P. Sun, Decay of Loschmidt Echo Enhanced by Quantum Criticality, *Phys. Rev. Lett.* **96**, 140604 (2006).
- [10] D. Rossini, T. Calarco, V. Giovannetti, S. Montangero, and R. Fazio, Decoherence induced by interacting quantum spin baths, *Phys. Rev. A* **75**, 032333 (2007).
- [11] F. M. Cucchietti, S. Fernandez-Vidal, and J. P. Paz, Universal decoherence induced by an environmental quantum phase transition, *Phys. Rev. A* **75**, 032337 (2007).
- [12] C. Cormick and J. P. Paz, Decoherence induced by a dynamic spin environment: The universal regime, *Phys. Rev. A* **77**, 022317 (2008).
- [13] W. H. Zurek, Quantum Darwinism, *Nat. Phys.* **5**, 181 (2009).
- [14] B. Damski, H. T. Quan, and W. H. Zurek, Critical dynamics of decoherence, *Phys. Rev. A* **83**, 062104 (2011).
- [15] T. Nag, U. Divakaran, and A. Dutta, Scaling of the decoherence factor of a qubit coupled to a spin chain driven across quantum critical points, *Phys. Rev. B* **86**, 020401(R) (2012).
- [16] S. Suzuki, T. Nag, and A. Dutta, Dynamics of decoherence: Universal scaling of the decoherence factor, *Phys. Rev. A* **93**, 012112 (2016).
- [17] E. Vicari, Decoherence dynamics of qubits coupled to systems at quantum transitions, *Phys. Rev. A* **98**, 052127 (2018).
- [18] E. Fiorelli, A. Cuccoli, and P. Verrucchi, Critical slowing down and entanglement protection, *Phys. Rev. A* **100**, 032123 (2019).
- [19] D. Rossini and E. Vicari, Scaling of decoherence and energy flow in interacting quantum spin systems, *Phys. Rev. A* **99**, 052113 (2019).
- [20] D. Rossini and E. Vicari, Coherent and dissipative dynamics at quantum phase transitions, *Phys. Rep.* **936**, 1 (2021).
- [21] M. Campostrini, A. Pelissetto, and E. Vicari, Finite-size scaling at quantum transitions, *Phys. Rev. B* **89**, 094516 (2014).
- [22] M. Campostrini, A. Pelissetto, and E. Vicari, Quantum transitions driven by one-bond defects in quantum Ising rings, *Phys. Rev. E* **91**, 042123 (2015); Quantum Ising chains with boundary fields, *J. Stat. Mech.* (2015) P11015.
- [23] M. Campostrini, J. Nespolo, A. Pelissetto, and E. Vicari, Finite-Size Scaling at First-Order Quantum Transitions, *Phys. Rev. Lett.* **113**, 070402 (2014); Finite-size scaling at first-order quantum transitions of quantum Potts chains, *Phys. Rev. E* **91**, 052103 (2015).
- [24] A. Pelissetto, D. Rossini, and E. Vicari, Finite-size scaling at first-order quantum transitions when boundary conditions favor one of the two phases, *Phys. Rev. E* **98**, 032124 (2018).
- [25] D. Rossini and E. Vicari, Ground-state fidelity at first-order quantum transitions, *Phys. Rev. E* **98**, 062137 (2018).
- [26] A. Pelissetto, D. Rossini, and E. Vicari, Dynamic finite-size scaling after a quench at quantum transitions, *Phys. Rev. E* **97**, 052148 (2018).
- [27] A. Pelissetto, D. Rossini, and E. Vicari, Out-of-equilibrium dynamics driven by localized time-dependent perturbations at quantum phase transitions, *Phys. Rev. B* **97**, 094414 (2018).
- [28] A. Pelissetto, D. Rossini, and E. Vicari, Scaling properties of the dynamics at first-order quantum transitions when boundary conditions favor one of the two phases, *Phys. Rev. E* **102**, 012143 (2020).
- [29] P. Di Francesco, P. Mathieu, and D. Sénéchal, *Conformal Field Theory* (Springer, New York, 1997).
- [30] H. Nishimori and G. Ortiz, *Elements of Phase Transitions and Critical Phenomena* (Oxford University Press, Oxford, 2011), Chap. 10.
- [31] T. W. Burkhardt and I. Guim, Finite-size scaling of the quantum Ising chain with periodic, free, and antiperiodic boundary conditions, *J. Phys. A: Math. Gen.* **18**, L33 (1985).
- [32] P. Pfeuty, The one-dimensional Ising model with a transverse field, *Ann. Phys. (NY)* **57**, 79 (1970).
- [33] G. G. Cabrera and R. Jullien, Universality of Finite-Size Scaling: Role of the Boundary Conditions, *Phys. Rev. Lett.* **57**, 393 (1986); Role of the boundary conditions in the finite-size Ising model, *Phys. Rev. B* **35**, 7062 (1987).
- [34] S. Rufo and M. A. Continentino, Heisenberg Ising-Kondo necklace model with transverse field for the heavy fermion compound URu₂Si₂, *J. Phys.: Condens. Matter* **30**, 445605 (2018).
- [35] A. Franchi, D. Rossini, and E. Vicari, Critical crossover phenomena driven by symmetry-breaking defects at quantum transitions, *Phys. Rev. E* **105**, 034139 (2022).
- [36] R. Islam, E. E. Edwards, K. Kim, S. Korenblit, C. Noh, H. Carmichael, G.-D. Lin, L.-M. Duan, C.-C. Joseph Wang, J. K.

- Freericks, and C. Monroe, Onset of a quantum phase transition with a trapped ion quantum simulator, *Nat. Commun.* **2**, 377 (2011).
- [37] S. Debnath, N. M. Linke, C. Figgatt, K. A. Landsman, K. Wright, and C. Monroe, Demonstration of a small programmable quantum computer with atomic qubits, *Nature (London)* **536**, 63 (2016).
- [38] J. Simon, W. S. Bakr, R. Ma, M. E. Tai, P. M. Preiss, and M. Greiner, Quantum simulation of antiferromagnetic spin chains in an optical lattice, *Nature (London)* **472**, 307 (2011).
- [39] H. Labuhn, D. Barredo, S. Ravets, S. de Léséleuc, T. Macrì, T. Lahaye, and A. Browaeys, Tunable two-dimensional arrays of single Rydberg atoms for realizing quantum Ising models, *Nature (London)* **534**, 667 (2016).
- [40] Y. Salathé, M. Mondal, M. Oppliger, J. Heinsoo, P. Kurpiers, A. Potonik, A. Mezzacapo, U. Las Heras, L. Lamata, E. Solano, S. Filipp, and A. Wallraff *et al.*, Digital Quantum Simulation of Spin Models with Circuit Quantum Electrodynamics, *Phys. Rev. X* **5**, 021027 (2015).
- [41] A. Cervera-Lierta, Exact Ising model simulation on a quantum computer, *Quantum* **2**, 114 (2018).